

# Nuclear Magnetic Resonance as a probe of nanometre-size orbital textures in magnetic transition metal oxides

G. Papavassiliou<sup>1</sup>, M. Pissas<sup>1</sup>, M. Belesi<sup>2</sup>, M. Fardis<sup>1</sup>, D. Stamopoulos<sup>1</sup>, A. Kontos<sup>1</sup>, M. Hennion<sup>3</sup>, J. Dolinsek<sup>4</sup>, J. P. Ansermet<sup>5,\*</sup>, and C. Dimitropoulos<sup>1,\*</sup>

<sup>1</sup>*Institute of Materials Science, NCSR, Demokritos, 153 10 Aghia Paraskevi, Athens, Greece*

<sup>2</sup>*Dept. of Physics, Ames Laboratory, Iowa State University, Ames, Iowa 50011*

<sup>3</sup>*Laboratoire Leon Brillouin, CEA-CNRS, CE-Saclay, 91191 Gif sur Yvette, France*

<sup>4</sup>*Josef Stefan Institute, Jamova 39, 61111 Ljubljana, Slovenia*

<sup>5</sup>*Dept. of Physics, University of Illinois, Urbana, Illinois 1801, USA\**

(Dated: June 21, 2018)

The study of strong electron correlations in transition metal oxides with modern microscopy and diffraction techniques unveiled a fascinating world of nanosize textures in the spin, charge, and crystal structure. Examples range from high  $T_c$  superconducting cuprates and nickelates, to hole doped manganites and cobaltites. However, in many cases the appearance of these textures is accompanied with "glassiness" and multiscale/multiphase effects, which complicate significantly their experimental verification. Here, we demonstrate how nuclear magnetic resonance may be uniquely used to probe nanosize orbital textures in magnetic transition metal oxides. As a convincing example we show for the first time the detection of nanoscale orbital phase separation in the ground state of the ferromagnetic insulator  $\text{La}_{0.875}\text{Sr}_{0.125}\text{MnO}_3$ .

PACS numbers: 75.47.Lx, 76.60.-k, 75.30.Et, 73.22.-f

It is widely accepted by now that orbital ordering is a key property, which controls the electronic behaviour of many transition metal oxides [1, 2, 3, 4]. A seminal case is  $\text{LaMnO}_3$  [5, 6], where at temperatures lower than  $T_{JT} \approx 780\text{K}$ , cooperative Jahn-Teller (JT) distortions force an antiferro-orbital ordering within the  $ab$  plane. This orbital arrangement defines the magnetic order of the ground state via the Goodenough-Kanamori-Anderson rules: Spins are coupled ferromagnetically in the  $ab$  planes and antiferromagnetically along the  $c$  axis, giving rise to the so called A-type antiferromagnetic (AFM) spin ordering. By substituting La with a divalent cation such as Sr, the JT-active  $\text{Mn}^{3+}$  sites are replaced by Jahn-Teller-inactive  $\text{Mn}^{4+}$  sites, thus introducing into the system holes and energizing ferromagnetic (FM) coupling through the double exchange mechanism [7]. New orbital structures are thus established [8, 9, 10, 11].

From the crystallographic perspective, by increasing doping  $x$  the ground state of the  $\text{La}_{1-x}\text{Sr}_x\text{MnO}_3$  (LSMO) changes from the JT distorted orthorhombic O' phase (canted AFM insulating), in the low doping regime, to the - almost cubic - orthorhombic O phase (FM and metallic) at  $x \approx 0.20$ , as shown in the lower pannel of Figure 1 [12, 13]. Around  $x \approx 0.125$  the system exhibits a peculiar FM and charge ordered (CO) ground state with nominally "pseudocubic" crystal structure, which is known in the literature as O" structure. The phase transition route for the  $x = 0.125$  system as a function of temperature is clearly seen in the SQUID and ac-susceptibility measurements, in the upper pannel of Figure 1. Three successive phase transitions are observed at temperatures  $T_{JT} \approx 283\text{K}$ ,  $T_c \approx 183\text{K}$ , and  $T_{CO} \approx 150\text{K}$ . The former transition (inset in the upper pannel of Figure 1) is related with the passage from the high temperature pseu-

docubic O phase to the JT-distorted O' phase [10, 14], while the latter marks the transition to the CO and orbitally reordered [10] O" phase. Besides, the large difference in the zero-field cooling and field cooling routes in the SQUID magnetization measurements is indicative of glassy freezing and metastability effects. Similar freezing effects have been observed in other Ca-doped manganites [15, 16], as well as in high  $T_c$  superconducting cuprates [17]. Most spectacularly, upon x-ray irradiation the charge ordered phase is partially destroyed below 40K, being restored only after heating above  $T_{CO}$  and subsequent cooling [18, 19]. The thermal history dependence of this effect and the observed photoinduced structural relaxation [18], indicates that the O" phase is extremely sensitive to the JT-induced strain fields, while showing a tendency to nanoscale phase separation [18]. Here, by using the NMR radiofrequency (rf) enhancement method [20], we uncover an important - but invisible until now - orbital phase separation in the ground state of  $x = 0.125$  LSMO. Specifically, we show that below 30K the FM and charge ordered O" matrix phase becomes unstable against the formation of FM nanodomains with the O-type orbital and crystal structure.

To show this intriguing orbital nanotexturing,  $^{139}\text{La}$  NMR rf enhancement measurements in zero external magnetic field were performed on three high quality LSMO single crystals, with doping  $x = 0.075, 0.125$ , and  $0.20$ . NMR in magnetic materials differs from conventional NMR techniques in several aspects [20]. The most obvious difference is the presence of a spontaneous magnetic hyperfine field,  $B_{hf} = \frac{1}{\gamma\hbar} A \langle S \rangle$  at the position of the resonating nuclei, where  $A$  and  $\langle S \rangle$  are the hyperfine coupling constant and the average electronic spin,

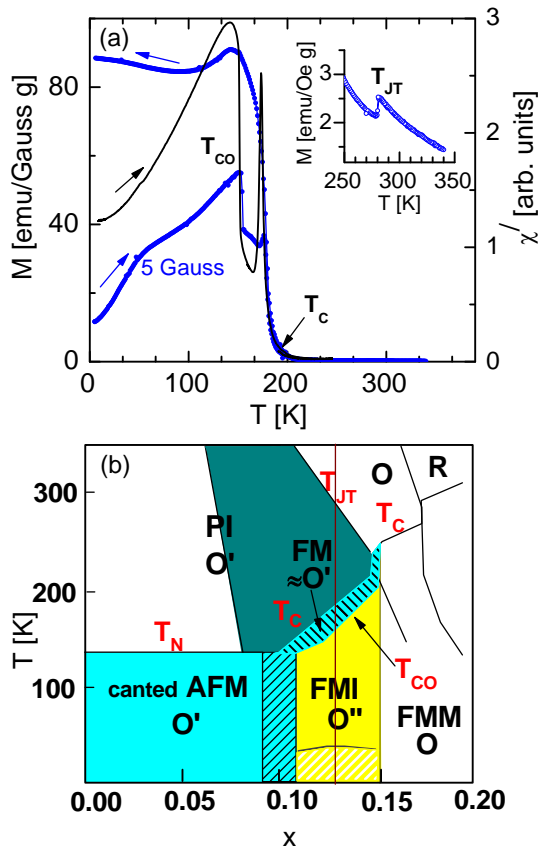


FIG. 1: The magnetic and structural phase transitions of  $\text{La}_{1-x}\text{Sr}_x\text{MnO}_3$  in the  $T-x$  region of interest. (a) SQUID magnetization measurements at 5 Gauss (blue curve), and ac-susceptibility measurements (black curve), performed on a high quality  $x = 0.125$  single crystal. (b) The  $T-x$  phase diagram, in the doping range  $0 \leq x \leq 0.2$ , as reconstructed from refs. [12, 13], by including magnetization and NMR data from the present work. The yellow-white hatched low temperature region around  $x = 0.125$  is characterized by nucleation of FM O-type nanodomains into the O' matrix. (FMI=FM insulating, FMM=FM metallic).

respectively. According to this formula, the hyperfine field  $B_{hf}(La)$  at the position of the spinless ( $S = 0$ ) La sites in LSMO compounds is expected to reflect the average spin state of the surrounding Mn octant, as well as possible deformations of the Mn-O-Mn bonding, which alter the hyperfine coupling constant  $A$  [15, 21]. A less apparent but very important difference is the existence of the rf enhancement [20, 21]. In FM materials, very strong NMR signals are produced at extremely low rf irradiation fields  $B_1$ , due to coupling of the rf field with the magnetic moments of the electrons. Specifically, the applied transverse rf field  $B_1$  produces an internal field  $B_1/(1 + N\chi)$ , where  $N$  is the demagnetizing factor, and  $\chi$  the magnetic susceptibility. The magnetization then rotates through an angle  $B_1/(1 + N\chi)B_A$ , where  $B_A$  is the magnetic anisotropy field. The rotation of the magnetization at the radiofrequency thus produces an effec-

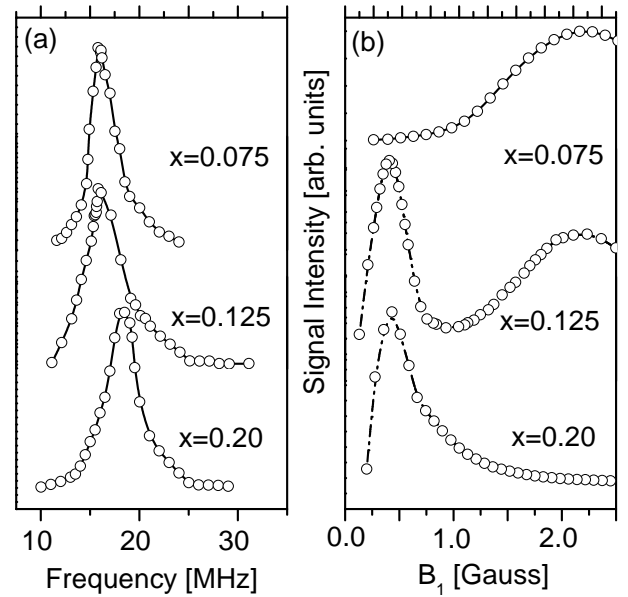


FIG. 2: (a) Zero field  $^{139}\text{La}$  NMR spectra of LSMO for  $x = 0.075, 0.125$ , and  $0.20$ , at  $5\text{K}$ . (b) The  $^{139}\text{La}$  NMR signal intensity  $I$  vs. the rf field  $B_1$  for  $x = 0.075, 0.125$ , and  $0.20$ .

tive rf field  $B_{1,eff}$  sufficiently stronger than the applied  $B_1$  by the factor  $n = [B_{hf}/(1 + N\chi)B_A]$ . We notice that the rf enhancement factor  $n$  would decrease in an external magnetic field, while at low fields both domain rotations and domain-wall displacements are expected to contribute to the transverse magnetization. However, in strongly inhomogeneous systems like CMR manganites, rf enhancement experiments reflect directly the local  $B_A$  in the various magnetic subphases [21].

Figure 2 shows zero field  $^{139}\text{La}$  NMR line shape measurements and rf enhancement plots at  $5\text{K}$  for the three systems under investigation. The line shapes were acquired by applying a two pulse spin-echo technique with pulse widths  $t_{p1} = t_{p2} = 0.6\mu\text{sec}$ , after recording the integrated spin-echo signal intensity  $I$  at successive irradiation frequencies. The rf enhancement experiments were performed by recording  $I$  as a function of the applied rf field  $B_1$ . The obtained  $I$  vs.  $B_1$  curves follow an asymmetric bell-shaped law with maximum at  $n\gamma B_1\tau = 2\pi/3$ , where  $\tau$  is the rf pulse duration,  $\gamma$  the nuclear gyromagnetic ratio, and  $n$  the rf enhancement factor [22]. According to the measurements no major changes are observed in the line shapes of the investigated samples, either with doping  $x$  (Figure 2a), or with temperature variation (not shown in the plot). Specifically, by increasing  $x$  the NMR spectra shift only slightly in frequency from  $\approx 16$  MHz for  $x = 0.075$  to  $\approx 18$  MHz for  $x = 0.20$ , indicating a nearly FM environment for the resonating nuclei in all three cases. The observation of FM NMR signals for  $x \geq 0.075$  is in agreement with "in field"  $^{139}\text{La}$  NMR line shape measurements for LSMO, with  $0 \leq x \leq 0.15$ , which show a very sharp changeover from the AFM to

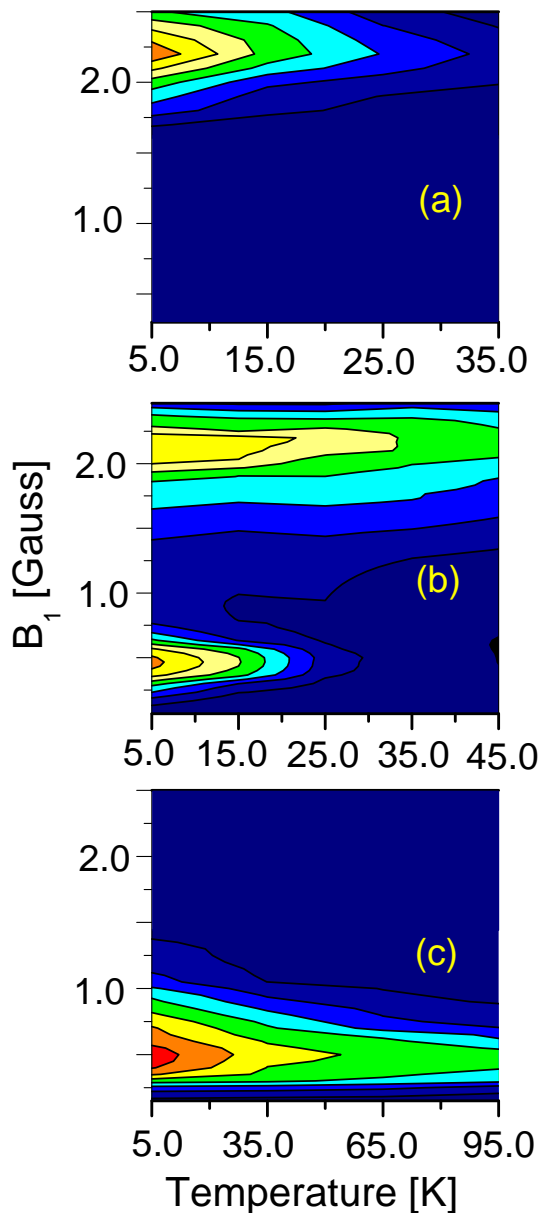


FIG. 3:  $^{139}\text{La}$  NMR rf enhancement experiments for  $\text{La}_{1-x}\text{Sr}_x\text{MnO}_3$  with (a)  $x = 0.075$ , (b)  $x = 0.125$ , and (c)  $x = 0.20$ . The contour plots show the NMR signal intensity  $I$  as a function of  $B_1$  and  $T$ . There is a significant difference in the rf enhancement by varying doping. The plot in the middle shows clearly that the ground state of the LSMO  $x = 0.125$  is a mixture of two phases differing in their magnetocrystalline anisotropy.

the FM phase at  $x \approx 0.05$  [23]. Besides, neutron scattering experiments have shown the presence of a single "FM modulated" canted AFM state for  $0.06 \leq x \leq 0.1$  [24, 25], comprised of FM plateletes, a few unit cells large on the  $ab$  plane, which are exchange coupled through the canted AFM matrix.

Contrary to the line shape measurements, a significant difference as a function of doping and temperature

is observed in the rf-enhancement experiments. According to Figure 2b the value  $B_{1,max}$ , where the maximum NMR signal is obtained, is shifted from 2.2 Gauss for  $x = 0.075$  (with the JT-distorted O' type crystal structure) to 0.5 Gauss for  $x = 0.20$  (with the orthorombic, and nearly isotropic O crystal structure). Most important, for  $x = 0.125$  the rf enhancement curve at 5K is a superposition of the corresponding curves for the  $x = 0.075$  and 0.20 systems, indicating the spontaneous splitting of the system in two phases with indistinguishable spin-structures, but different magnetocrystalline anisotropy. The evolution of this exciting phase separation by varying temperature can be nicely followed in the contour plots of Figure 3. For  $T > 30\text{K}$  a single phase is observed in Figure 3b, which can be attributed to the O'' structure with antiferro-orbital ordering [26], while at  $T \leq 30\text{K}$  a second phase component appears, resembling the O structure of the  $x = 0.20$  system. We stress that synchrotron X-rays diffraction experiments observe only O''-type nanodomains with average size  $\approx 30 - 35$  nm [18]. Evidently, the O-type phase component is confined into smaller "invisible" regions, which increase in size and become detectable only after strong illumination with X-rays [18]. The nucleation of such O-type islands explains the fast decrease of the antiferro-orbital ordering, observed with resonant X-ray scattering experiments in the low temperature regime of the O'' phase [26]. It is also worth to notice the similarity in the contour plots of the O' and O'' phases. A possible explanation is that at low doping, such as  $x = 0.075$ , the observed NMR signals are solely produced in FM plateletes [24, 25] which are precursors of the O'' phase. However, the size ( $\approx 2$  nm) and the strong coupling of such plateletes with the canted AFM matrix state [24, 25], suggests that their anisotropy should be rather determined by the anisotropy of the O' matrix state. It is thus possible that despite the different orbital hybridization of the O' and O'' phases, the similarity in their orbital ordering (i.e. antiferro-orbital ordering for both phases [26]) gives rise to comparable  $B_A$  values.

Further information about this orbital phase separation, has been obtained by performing  $^{139}\text{La}$  NMR spin-spin relaxation time ( $T_2$ ) measurements on both phase components.  $T_2$ s were measured with the two pulse spin-echo technique, as previously described, by varying the time interval between the two pulses and recording the decay of the spin-echo signal intensity. The experimental data in Figure 4 show that the appearance of the O phase component is accompanied with a slope change in the  $T_2$  vs.  $T$  curve of the O'' phase component. Most important, below 30K the  $T_2$  curves for both phase components exhibit the same slope, which is indicative of a similar evolution in their spin dynamics by cooling. Hence, the picture that emerges from Figures 3 and 4 is that the O'' phase is metastable, whereas below 30K droplets of the O phase at nanometer-scale start to nucleate. A possi-

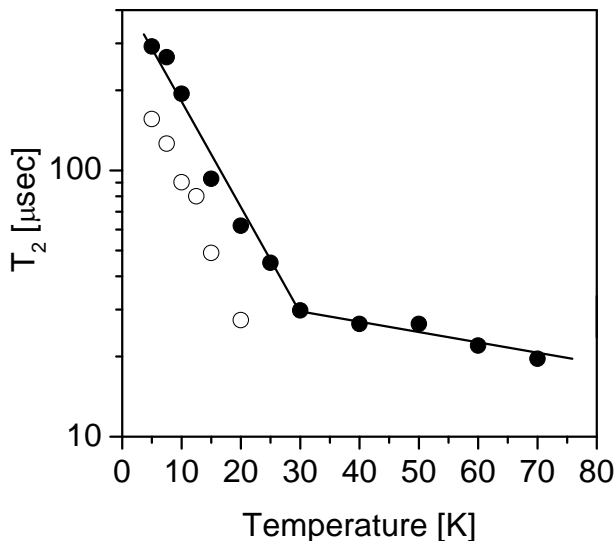


FIG. 4:  $^{139}\text{La}$  NMR spin-spin relaxation time  $T_2$  of  $\text{La}_{0.875}\text{Sr}_{0.125}\text{MnO}_3$  as a function of temperature. Measurements were performed at two different rf fields, i.e. at  $B_1 = 0.5$  Gauss (open circles) and 2.2 Gauss (filled circles), which correspond to signals from the O and O' structures, respectively. It is observed that the appearance of O-type domains is accompanied with a slope change in the  $T_2$  of the signal from the O' domains.

ble explanation for this behaviour is that strain fields, characterizing the JT-distorted O' phase, are decreasing gradually in the O'' phase, giving rise to undistorted FM metallic islands below a certain transition temperature. A new region, is thus defined in the  $T-x$  phase diagram, which is shown as yellow-white hatched region in Figure 1.

In summary, the direct relation between  $B_A$  and the NMR rf enhancement in low doped LSMO, allowed us to unveil an unexpected orbital nanophase separation in the ground state of LSMO,  $x = 0.125$ . This kind of phase separation appears to underlie to the photoinduced phase segregation in LSMO [18], as well as in other CMR manganites [27]. In general, the method we have employed here is applicable in many other magnetic transition metal oxides, where orbital rearrangements are not reflected on the spin structure, but give appreciable dif-

ferences in the local magnetocrystalline anisotropy.

---

\* Institut de Physique Experimentale, EPFL-PH-Ecublens, 1015-Lausanne, Switzerland

- [1] Y. Tokura and N. Nagaosa, *Science* **288**, 462 (2000).
- [2] E. Saitoh, *et al.*, *Nature* **410** 180 (2001).
- [3] E. Dagotto, T. Hotta, A. Moreo, *Phys. Rep.* **344**, 1 (2001).
- [4] T. Hotta, E. Dagotto, *Phys. Rev. Lett.* **92**, 227201 (2004).
- [5] J. Rodriguez-Carvajal, *et al.*, *Phys. Rev. B* **57**, R3189 (1998).
- [6] Y. Murakami, *et al.*, *Phys. Rev. Lett.* **81**, 582 (1998).
- [7] P.G. de Gennes, *Phys. Rev.* **118**, 141 (1960).
- [8] Y. Yamada, *et al.*, *Phys. Rev. Lett.* **77**, 904 (1996).
- [9] J. Deisenhofer, *et al.*, *Phys. Rev. B* **68**, 214427 (2003).
- [10] J. Geck, *et al.*, *Phys. Rev. B* **69**, 104413 (2004).
- [11] T. Mizokawa, D. I. Khomskii, and G. A. Sawatzky, *Phys. Rev. B* **61**, R3776 (2000).
- [12] M. Paraskevopoulos, *et al.*, *J. Phys.: Condens. Matter* **12**, 3993 (2000).
- [13] G.-L. Liu, J.-S. Zhou, and J. B. Goodenough, *Phys. Rev. B* **64**, 144414 (2001).
- [14] S. Uhlenbruck, *et al.*, *Phys. Rev. Lett.* **82**, 185 (1999).
- [15] G. Papavassiliou, M. Belesi, M. Fardis and C. Dimitropoulos, *Phys. Rev. Lett.* **87**, 177204 (2001).
- [16] V. Markovich, *et al.*, *Phys. Rev. B* **70**, 064414 (2004).
- [17] M. H. Julien, *et al.*, *Phys. Rev. B* **63**, 144508 (2001).
- [18] V. Kiryukhin, Y. J. Wang, F. C. Chou, M. A. Kastner, R. J. Birgeneau, *Phys. Rev. B* **59**, R6581 (1999).
- [19] D. Casa, *et al.*, *Phys. Rev. B* **64**, 100404(R) (2001).
- [20] A. C. Gossard and A. M. J. Portis, *Phys. Rev. Lett.* **3**, 164 (1959); P. Panissod, C. Meny, *Appl. Mag. Reson.* **19**, 447 (2000).
- [21] G. Papavassiliou, *et al.*, *Phys. Rev. Lett.* **91**, 147205 (2003).
- [22] G. Papavassiliou *et al.*, *Phys. Rev. B* **55**, 15000 (1997).
- [23] K. Kumagai, *et al.*, *Phys. Rev. B* **59**, 97 (1999).
- [24] M. Hennion, *et al.*, *Phys. Rev. B* **61**, 9513 (2000).
- [25] P. Kober-Lehouelleur, *et al.*, *Phys. Rev. B* **70**, 144409 (2004).
- [26] Y. Endoh, *et al.*, *Phys. Rev. Lett.* **82**, 4328 (1999).
- [27] K. Miyano, T. Tanaka, Y. Tomioka, and Y. Tokura, *Phys. Rev. Lett.* **78**, 4257 (1997).